Thermodynamics and Exchange Stiffness of Asymmetrically Sandwiched Ultrathin Ferromagnetic Films with Perpendicular Anisotropy

Ivan A. Yastremsky,[1,2,†] Oleksii M. Volkov,[2] Martin Kopte,[2] Tobias Kosub,[2] Sven Stienen,[2] Kilian Lenz,[2] Jürgen Lindner,[2] Jürgen Fassbender,[2] Boris A. Ivanov,[1,3,4] and Denys Makarov[2,*]

[1] *Taras Shevchenko National University of Kyiv, 01601 Kyiv, Ukraine*

[2] *Helmholtz-Zentrum Dresden - Rossendorf e.V., Institute of Ion Beam Physics and Materials Research, Bautzner Landstrasse 400, 01328 Dresden, Germany*

[3] *Institute of Magnetism, National Academy of Sciences and Ministry of Education and Science, 03142 Kyiv, Ukraine*

[4] *National University of Science and Technology "MISiS", Moscow 119049, Russian Federation*

(Received 30 July 2019; revised manuscript received 29 October 2019; published 16 December 2019)

Thermodynamic properties, in particular, the temperature dependencies of magnetization of asymmetrically sandwiched ultrathin cobalt films with perpendicular anisotropy are investigated. The experimental results are described theoretically in the frame of magnon thermodynamics consistently accounting for the finite thickness of the films. The analysis includes both three-dimensional (Bloch's $T^{3/2}$ law) and two-dimensional (the 2D Bloch law) theories as limiting cases. By fitting the experimental temperature dependencies of magnetization to the theoretical model, the exchange stiffness parameter is extracted. This approach provides access to the exchange stiffness without the need to know the strength of the Dzyaloshinskii-Moriya interaction in the stack. The exchange stiffness of sub-nm-thick Co films is found to be about three times smaller compared to the case of bulk cobalt. In the temperature range $T < 170 \pm 30$ K the temperature dependencies of magnetization follow the 2D Bloch law. The applicability of Bloch's $T^{3/2}$ law and analysis of the Curie temperature (two-dimensional and three-dimensional pictures) to extract the exchange stiffness for sub-nm-thick Co films are tested as well. The closest value of the exchange stiffness to the magnon thermodynamics turned out to be within the analysis of the Curie temperature in the three-dimensional picture.

DOI: 10.1103/PhysRevApplied.12.064038

I. INTRODUCTION

Ultrathin magnetic films resemble a versatile playground to study fundamentals of low-dimensional magnetism including the possibility to observe a crossover between three-dimensional (3D) and two-dimensional (2D) behavior. Recently, the focus was shifted to asymmetrically sandwiched ferromagnetic ultrathin films with perpendicular magnetic anisotropy and interface-induced Dzyaloshinskii-Moriya interaction (DMI), which can support chiral magnetic textures including magnetic skyrmions [1–3], skyrmion bubbles [4], or chiral magnetic domain walls [5]. These objects promise to become new fundamental units for logic and memory devices. The performance of these devices, e.g., storage density and the operation speed is determined by the physical nature of the specific type of the chiral object. This, in turn, imposes stringent requirements on the functional magnetic layer whose micromagnetic properties should be precisely known to identify the type of the chiral object of being either skyrmion or skyrmion bubble. The type of the chiral object is determined by the micromagnetic parameters of the material, i.e., saturation magnetization, anisotropy energy, exchange parameter, and DMI strength. Major advances were achieved by demonstrating room-temperature skyrmions and skyrmion bubbles in asymmetrically sandwiched Co thin films featuring interface-induced DMI [6,7]. The type of magnetic object, its fundamental properties (like size and mobility) as well as its responses to external stimuli are given by the intrinsic magnetic parameters. Given the extreme thinness of the Co layer typically below 1 nm, the micromagnetic parameters of these technologically relevant asymmetric ferromagnetic sandwiches differ substantially compared to their respective bulk values. While magnetization and anisotropy can be determined from regular integral measurements, the exchange stiffness as well as the DMI constant are more difficult to be measured. One of the challenges is that these two parameters are often interlinked and the determination of one of them implies the precise knowledge of the other one.

*d.makarov@hzdr.de
†yastremsky@ukr.net

The exchange stiffness, A, can be extracted from the spin-wave dispersion law. However, surface-sensitive techniques for analyzing the spin-wave dispersion, such as inelastic scanning tunneling spectroscopy [8], spin-polarized electron-energy-loss spectroscopy [9] can hardly be used for magnetic sandwiches, where the magnetic film is covered with functional layers. In ultrathin magnetic films with perpendicular magnetic anisotropy A can be deduced from the spectroscopy of electrically pumped spin waves in circular magnetic tunnel-junction nanopillars [10]. Techniques, based on neutron scattering [11], magneto-optical measurements [12,13], inelastic x-ray scattering [14], Brillouin light scattering [15], and broadband ferromagnetic resonance using inductive methods [16,17] are successfully applied to study thin films but still possess difficulties in determining exchange stiffness of ultrathin films. Methods, based on the analysis of magnetic domain patterns require the knowledge of the DMI constant and are also sensitive to the presence of the structural disorder [18–21]. For 3D samples, the exchange stiffness is often determined through the analysis of the temperature dependence of magnetization within the spin-wave approach, where Bloch's $T^{3/2}$ law is well established. However, for ultrathin films the thermal dependence of the magnetization is very sensitive to the range of the interactions, size, and shape of the system [22–26], which have to be taken into account. The investigation of the thermodynamic properties of low-dimensional magnets allows for the determination of the intrinsic parameters, which are hard to measure by standard methods, typically applicable for thicker magnetic films. This ambiguity in the value of the exchange parameter has severe consequences on the experimentally deduced DMI strength especially when relying on the widely used quasistatic approaches, e.g., based on the analysis of the asymmetric domain-wall growth studied using Kerr microscopy measurements. This deficiency limits the possibility to compare the data reported by different groups even if it is taken for the nominally same magnetic system.

Here, the results of the theoretical and experimental analysis of ultrathin Co films with asymmetric interfaces (one heavy metal, Pt, and one nonmagnetic metal oxide, CrO_x) are reported. The temperature dependencies of the magnetization are measured and analyzed theoretically based on the magnon-gas approach applied to magnetic films of finite thickness (in the following refereed to as the rigorous approach). The best fit to the experimental data up to room temperature is obtained within a quasi-two-dimensional model, accounting for the lowest transversal spin-wave mode. The 2D Bloch law is applicable as well but only in the limited temperature range of $T < 170 \pm 30$ K. At the same time, fitting the experimental data to Bloch's $T^{3/2}$ law provides a twice smaller value of the exchange stiffness compared to the rigorous approach. The analysis of the Curie temperature (2D and 3D pictures) to extract the exchange stiffness for sub-nm-thick Co films are tested to extract the exchange stiffness as well. The closest value of the exchange stiffness to the rigorous approach turned out to be within the analysis of the Curie temperature in the 3D picture.

II. THERMODYNAMIC MODEL

The energy density of asymmetrically sandwiched ultrathin ferromagnetic films with perpendicular anisotropy and interface-induced DMI writes as Ref. [27]

$$E = A(\nabla \mathbf{m})^2 - Km_z^2 + D[m_z \operatorname{div} \mathbf{m} - (\mathbf{m} \cdot \nabla)m_z], \quad (1)$$

where A is the exchange stiffness, $\mathbf{m} = \mathbf{M}/M$ is a unit magnetization vector, $M = |\mathbf{M}|$ is a modulus of the magnetization, K is a constant of the effective easy-axis anisotropy (including the demagnetizing field effects in the local approximation), D is the DMI constant and the z axis is perpendicular to the sample plane. For the theoretical description, a thermodynamic model is constructed based on the approach of a noninteracting magnon gas. Note, both nonlinear (solitons) [28,29] and linear (magnons) excitations could contribute to the physics of low-dimensional magnets. However, the solitonic contribution can be safely excluded for sub-nm-thick magnetic films. Indeed, solitonic excitations in a one-monolayer-thick film have an energy of the order of the exchange integral per one atomic plane. Hence, for ultrathin films containing several planes, their energies are too high to be excited at temperatures lower than the Curie temperature. Thus, only the magnon thermodynamics are an adequate approach for the calculation of the thermodynamical parameters of such samples.

Asymmetrically sandwiched ultrathin ferromagnetic films with perpendicular anisotropy typically possess strong surface-induced DMI [30–32]. The DMI-induced effective magnetic field is $\mathbf{H}_{\mathrm{DMI}} = (2D/M)(\partial m_z/\partial x; \partial m_z/\partial y; -\operatorname{div} \mathbf{m})$. In the case, when the magnetization is perpendicular to the sample plane, only nonlinear corrections of the amplitude of spin waves enter the Landau-Lifshitzh equation. These nonlinear corrections can be neglected when describing dynamics of spin waves with small amplitudes ($m_x \sim m_y \ll 1$).

For sufficiently low temperatures, the change of magnetization with temperature can be calculated through the magnon density $\langle n \rangle$ as follows [33–35]: $\Delta M(T) = M(0) - M(T) = g\mu_B \langle n \rangle / L_x L_y t$, where g is the Landé factor, $\langle n \rangle = \sum_{\mathbf{k}} n_{\mathbf{k}}$ is the average number of magnons in the sample, $\mathbf{k}$ is a wave vector ($k = |\mathbf{k}|$), $n_{\mathbf{k}} = 1/\{\exp[\hbar\omega(k)/(k_B T)] - 1\}$ is the magnon occupation number, T is the temperature, $\omega(k)$ describes the magnon dispersion law, k_B is the Boltzmann constant, L_x and L_y denote the lateral size of the sample, and t is thickness of the ferromagnetic layer. The summation is performed over

all magnon eigenstates within the first Brillouin zone. The electron spin is assumed to be the only source of magnetic moment in ultrathin ferromagnetic films. Furthermore, sufficiently low temperatures are considered, such that excitations of magnons at the edge of the first Brillouin zone, where the dispersion law is not parabolic, can be neglected. Thus, for the chosen geometry with **M** perpendicular to the sample plane, the dispersion law has no contribution from the DMI and in the long-wave approximation is parabolic $\omega(k) = \omega_0 + 2\gamma(A/M)k^2$, where ω_0 is a gap in the magnon spectrum, γ is the gyromagnetic ratio. For the modeling of the spin-wave spectra of the samples free-boundary conditions are used. For free boundary the homogeneous ferromagnetic resonance mode with the frequency ω_0 exists. Then the set of wave vectors of magnon eigenstates is $k_i = \pi n_i/L_i$, with $n_i = 0, 1, 2, \ldots, N_i - 1$, where $i = \{x, y, z\}$ (here $L_z = t$) and N_i is the number of magnetic layers along the ith axis. For small t of the order of a few monolayers, the sample supports only a few transversal eigenmodes. Thus, for a consistent description of the thermodynamics of ultrathin films, it is convenient to present the temperature change of the magnetization as a sum over these transversal modes,

$$\Delta M = M(0) - M(T) = \sum_{n_z} \Delta M_{n_z}, \tag{2}$$

where ΔM_{n_z} is a contribution to ΔM of magnon states within the branch of fixed n_z in a reciprocal space. ΔM_0 is responsible for the strict 2D behavior, $\Delta M_1, \Delta M_2 \ldots$ determine effects of non-two-dimensionality. A relative contribution of the transversal modes with ($n_z \geqslant 1$) to $\langle n \rangle$ can be considered as a rate of deviation of the magnetic properties of the film from the strict 2D behavior. The lateral size of the samples are of the order of millimeters. Therefore, when estimating ΔM_{n_z}, the summation can be replaced by integration. The spectral density of magnon states within the plane with fixed n_z is expressed by $D = L_x L_y M/(8\pi\gamma A)$, which is independent of ω and n_z. Then, the analytical expression for ΔM_{n_z} can be written as follows:

$$\Delta M_{n_z} = \frac{\mu_B M}{4\pi\gamma A t} \frac{k_B T}{\hbar} \ln\left[\frac{\exp(\hbar\omega_{n_z}/k_B T)}{\exp(\hbar\omega_{n_z}/k_B T) - 1}\right]. \tag{3}$$

Here, $\omega_{n_z} = \omega(\pi\, n_z/t)$ is the lowest frequency within the n_zth branch. For sufficiently thick films, ΔM converges to Bloch's $T^{3/2}$ law (3D case, Appendix A)

$$\Delta M_{3D} = 2\mu_B \times 0.0587 \times \left(\frac{k_B T M}{2\gamma\hbar A}\right)^{3/2}. \tag{4}$$

The temperature at which ΔM_{n_z} gives a considerable contribution can be defined as $T_{n_z} = \hbar\omega_{n_z}/k_B$. The activation temperature of the gap T_0 is of the order of several kelvin. For $T < T_1$, the terms with $n \geqslant 1$ in Eq. (2) can be neglected and for $T > T_0$, ΔM is reduced to the 2D Bloch law [35,36]

$$\Delta M_0 = \frac{\mu_B M}{4\pi\gamma A t} \frac{k_B T}{\hbar} \ln\left[\frac{k_B T}{\hbar\omega_0}\right] \tag{5}$$

and the system can be considered as strictly two dimensional. It should be noted that when $\omega_0 \to 0$, the density of magnons with small wave vectors diverges and thus, ΔM_0 diverges [33]. This divergence is a consequence of the Mermin-Wagner theorem known for isotropic two-dimensional ferromagnets [36]. For higher branches ΔM_{n_z} remains finite even for $\omega_0 \to 0$. The activation temperature T_{n_z} increases with n_z. Thus, the strongest contribution is given by ΔM_0 while ΔM_{n_z} decreases for higher n_z. For $T \gg T_0$, ΔM_0 depends almost linearly on T.

The numerical modeling of ΔM at fixed exchange stiffness demonstrates that ΔM is a monotonically decaying function of the film thickness. For a monolayer magnetic film ΔM is equal to the 2D Bloch law. For sufficiently large film thickness ΔM converges to Bloch's $T^{3/2}$ law. This decay of ΔM is consistent with the fact that, according to the Mermin-Wagner theorem, 3D ferromagnets are more stable against thermal fluctuations than 2D ferromagnets.

III. EXPERIMENTAL VALIDATION

To validate the developed theory, a series of asymmetric Co sandwiches is fabricated by magnetron sputtering (argon sputter pressure of 10^{-3} mbar) at room temperature on thermally oxidized Si wafers. The layer stack consists of //CrO_x(5 nm)/Co($t = 0.6, 0.7, 0.8, 0.9$ nm)/Pt(2 nm) trilayers. The methodology for measuring the film thickness is as follows. First, the deposition rate for each deposited material is calibrated. For doing this, thin films of a certain thickness are deposited and the time required for the deposition is noted. The final deposited thickness is calibrated using x-ray reflectivity measurements. The deposition rate is calculated by knowing the measured thickness and respective deposition time. The calibrated deposition rate is then consistently used to prepare all samples from the series. The samples are characterized using transport and integral magnetometry to determine the temperature dependence of the magnetization $M(T)$ in the range from 5 to 400 K. By measuring hard-axis hysteresis loops, the effective anisotropy field H_K (accounting for the shape anisotropy) at room temperature can be accessed. All samples demonstrate strong perpendicular anisotropy with out-of-plane easy axis of magnetization [Fig. 1(a)] and sizeable DMI [21]. The $M(T)$ dependencies of these samples are presented in Fig. 1(b). Within the theory of critical phenomena the $M(T)$ dependencies for temperatures close

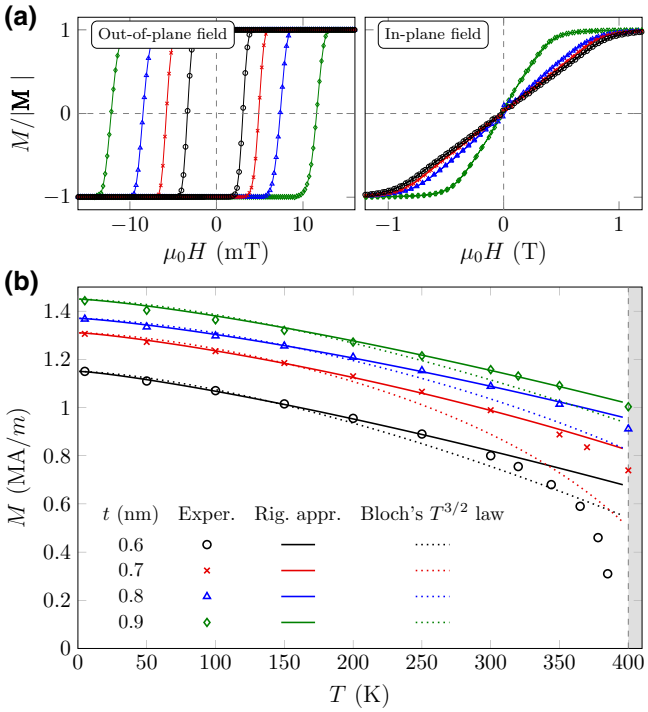

FIG. 1. (a) Magnetic hysteresis loops of //CrO_x/Co(t)/Pt samples measured at 300 K with the external magnetic field applied along the easy (out-of-plane) and hard (in-plane) axis. (b) Temperature dependence of the magnetization, $M(T)$. Symbols denote experimental data. Solid lines are fits according to Eq. (2), i.e., the rigorous approach, "Rig. appr.". Dotted lines are fits to Bloch's $T^{3/2}$ law [Eq. (4)].

to T_C follow the universal law [37]

$$M(T) = M(0)\left(1 - \frac{T}{T_C}\right)^{\beta}, \tag{6}$$

where β is the critical exponent. There are two fitting parameters, T_C and β. Only for the sample with 0.6-nm Co thickness the Curie temperature lies within the accessible measurement range of 400 K. For this sample the theory of critical phenomena can therefore be applied rigorously. For the other samples with $t > 0.6$ nm, T_C is outside the measured region. Still, for the estimation of T_C, the same procedure is used where the analytical expression $M(T)$ is matched to the experimental data at $T =$ 400 K. The corresponding estimations of T_C are marked with * in Table I, which also contains the information on the thickness dependence of the saturation magnetization and effective anisotropy field.

Furthermore, by performing X-band ferromagnetic resonance (FMR) cavity measurements, it is demonstrated that the minimal frequency, which is realized in the system, corresponds to the ferromagnetic resonance mode $\omega_0 = \gamma\,(\mu_0 H_K)$ (Appendix B). For the specific calculations the gyromagnetic ratio $\gamma = 1.63 \times 10^{11}$ rad/(sT)

TABLE I. Experimentally determined magnetic parameters of //CrO_x/Co(t)/Pt samples. The Curie temperatures T_C of the sample with $t = 0.6$ nm is determined within the theory of critical phenomena. For other samples, the T_C is estimated within the same model (indicated with *). For comparison, the Curie temperature of bulk Co is $T_C^b = 1394$ K.

t (nm)	$M(0)$ (MA/m)	H_K (MA/m)	T_C (K)
0.6	1.15	0.84	385
0.7	1.31	0.76	440*
0.8	1.37	0.70	479*
0.9	1.45	0.40	530*

is taken (Appendix B). Hence, the zero-field resonance frequency can be calculated using the experimentally measured effective anisotropy field $\omega_0 = \gamma\,(\mu_0 H_K)$ ($\omega_0 = 1.72 \times 10^{11}$, 1.56×10^{11}, 1.43×10^{11}, and 0.82×10^{11} rad/s for film thicknesses $t = 0.6$, 0.7, 0.8, and 0.9 nm, respectively).

The developed thermodynamical model based on the spin-wave approach is applied for the description of the experimentally measured temperature dependencies of magnetization of //CrO_x/Co(t)/Pt films, Fig. 1(b). For the modeling of the samples with $t = 0.6, 0.7, 0.8, 0.9$ nm, the number of magnetic monolayers is $N_z = 4, 5, 6, 7$, respectively. The best fit is performed to the experimental data in the temperature range of up to 200 K. In this range, the amplitudes of spin waves are small and the approximation of a noninteracting magnon gas is valid. The values of the magnon gap are taken from the calculated values $\omega_0 = \gamma\,(\mu_0 H_K)$. The exchange stiffness A is the only fitting parameter of the model. The result of this fitting procedure is presented in Fig. 1(b) by solid lines. Almost up to room temperature, the theory matches the experimental data. The values of A, corresponding to the best-fit procedure, are summarized in Table II in the column indicated as "Rig. appr.".In line with previous studies [10,26], a substantial reduction of A is found with the decrease of the film thickness compared to bulk cobalt ($A^b \approx 16$ pJ/m). For the obtained values of A, the activation temperature for the mode with $n_z = 1$ is $T_1 \approx 170 \pm 30$ K (for higher modes T_{n_z} is higher than T_C). Therefore, practically, only two modes, M_0 and M_1, are relevant for the case of //CrO_x(5 nm)/Co(0.6 − 0.9 nm)/Pt(2 nm) samples. The comparison of the experimental and theoretical ΔM dependencies (Fig. 2) reveals that the accuracy of the fit increases when accounting for transversal modes, especially for thicker samples. For $T < T_1$ the contribution of the transversal modes can be neglected. However, for higher temperatures, the relative contribution of ΔM_1 increases and reaches about 7%–15% at room temperature. The discussion of the impact of the temperature dependence of the exchange stiffness on the fitting of the experimental $M(T)$ data is presented in Appendix C.

TABLE II. Estimation of the exchange stiffness A based on different approaches: rigorous approach, Bloch's $T^{3/2}$ law and the Curie temperature T_C within the 3D and 2D pictures. Note, the estimation of A from T_C within the 2D picture is performed within a model of a single atomic layer with a square spin lattice. For an fcc structure these estimations should be multiplied by about 3. For comparison, the exchange stiffness of bulk cobalt, $A^b \approx 16$ pJ/m.

t (nm)	A (pJ/m)			
	Rig. appr.	Bloch's $T^{3/2}$ law	T_C (3D)	T_C (2D)
0.6	6.3	2.9	4.4	8.3
0.7	6.9	3.4	5.0	10.6
0.8	7.3	3.8	5.4	11.9
0.9	6.8	3.7	6.0	14.7

In the following, the applicability of Bloch's $T^{3/2}$ law to estimate A in //CrO_x(5 nm)/Co(0.6 − 0.9 nm)/Pt(2 nm) trilayers is tested. The fitting procedure is performed within the same temperature range, as for the case of the rigorous approach. The extracted values of A are presented in Table II in the column indicated as "Bloch's $T^{3/2}$ law". The exchange stiffness A is found to be about twice smaller than within the rigorous approach. Numerically calculated temperature dependencies, obtained based on Bloch's $T^{3/2}$ law are presented in Figs. 1(b) and 2. Bloch's $T^{3/2}$ law provides a worse description of the experimental data compared to the rigorous approach. To understand this reduction of A we note that Bloch's $T^{3/2}$ law gives a smaller value of the change of magnetization (ΔM_{3D}) than ΔM calculated within the rigorous approach of films with finite thickness. Thus, to compensate for the larger experimentally observed value of ΔM, the model effectively reduces the exchange stiffness.

The exchange stiffness can be evaluated from its correlation to the Curie temperature, T_C. Two limiting cases are considered, i.e., specific for 3D and 2D systems. For the 3D picture in the first approximation A is proportional to T_C. The proportionality coefficient depends on a specific system and requires elaborate calculations. For the estimation of A in //CrO_x(5 nm)/Co(0.6 − 0.9 nm)/Pt(2 nm) trilayers, the same value of the proportionality coefficient as for bulk Co is used. For known A^b and the Curie temperature of bulk Co ($T_C^b = 1394$ K), the thickness scaling of the exchange parameter can be written as $A(t) = A^b T_C(t)/T_C^b$, where $T_C(t)$ is the Curie temperature measured for the sample with the Co thickness t. The results are presented in Table II in the column indicated "T_C (3D)". The estimates of A are in reasonable agreement with the rigorous approach. Within the 2D picture, the exchange integral J [exchange energy between two spins $\mathbf{S_1}$, $\mathbf{S_2}$ is defined as $-2J(\mathbf{S_1}\mathbf{S_2})$] can be found from the relation between the Curie temperature and parameters of a one-monolayer-thick ferromagnetic film with perpendicular anisotropy [38]

$$k_B T_C = \frac{4\pi(S+1)}{3} \frac{2JS}{\ln(4\pi 2JS/\hbar\omega_0)}. \tag{7}$$

The effective spin per atom S is estimated assuming an fcc lattice with a nearest distance between atoms $a = 0.25$ nm (as in bulk Co) from the relation $M(0) = \sqrt{2}\mu_B S/a^3$. The result of this estimation is presented in Table III (column indicated "S"). S increases for thicker films and for the sample with $t = 0.9$ nm is about 8% lower than the

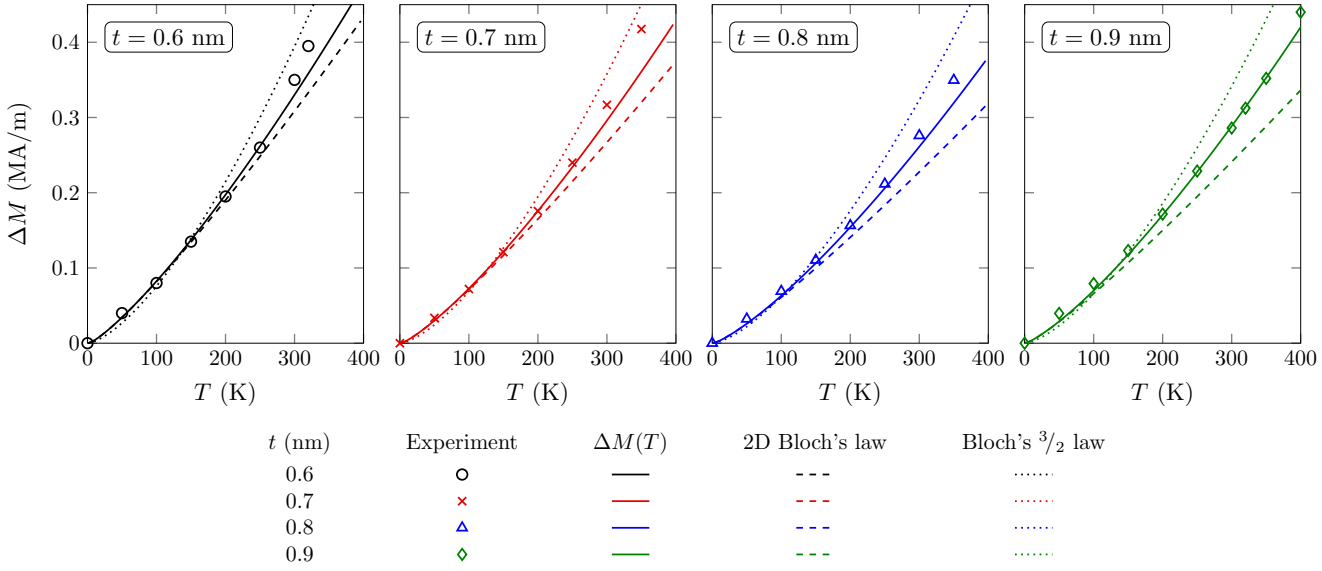

FIG. 2. Experimental (symbols) and theoretical (lines) temperature dependencies of ΔM for different film thicknesses. ΔM is plotted following the rigorous approach.

TABLE III. Estimation of the exchange integral J and effective spin per atom S. For comparison, the exchange integral and spin of bulk cobalt, $J^b/k_B \approx 155$ K, $S^b \approx 0.86$.

t (nm)	S	J/k_B (K)			
		Rig. appr.	Bloch's $T^{3/2}$ law	T_C (3D)	T_C (2D)
0.6	0.63	99	45	69	371
0.7	0.72	83	40	60	364
0.8	0.75	81	42	60	378
0.9	0.79	68	37	60	421

bulk value $S^b \approx 0.86$. For the known T_C, ω_0, and S, the computed values of J are presented in Table III [column indicated "T_C (2D)"] and are about 2.5 times larger than in bulk Co, $J^b/k_B \approx 155$ K [39]. To recalculate this parameter in A [40], a square spin lattice with a lattice constant $a = 0.25$ nm is assumed. The calculated values of $A \approx JS^2/a$ are found to be about twice higher than within the rigorous approach but lower than in bulk Co [Table II, column indicated "T_C (2D)"]. However, as the samples have several atomic layers, the number of nearest spins is higher than in the case of a single atomic layer. Consequently, A is expected to increase. For example, supposing an fcc structure, A increases by $2\sqrt{2}$ (about three) times and becomes about two times larger than for bulk Co. This overestimate of A and J is a consequence of the fact that two-dimensional ferromagnets are less stable against thermal fluctuations than three-dimensional ferromagnets. Therefore, a larger value of A (stronger exchange interaction J) is required to support the ferromagnetic order.

It is instructive to estimate the exchange integral relying on the obtained data for the exchange stiffness (Table II) within the rigorous approach, Bloch's $T^{3/2}$ law, and the Curie temperature T_C within the 3D picture. Assuming an fcc lattice and accounting for the nearest spins only, J is computed from the relation $A = 2\sqrt{2}JS^2/a$, where A is taken from Table II and S is taken from Table III. The result of this estimation is presented in Table III. The exchange integral deduced from the rigorous approach is about twice smaller than in bulk Co. Analogously to the exchange stiffness, the closest value of the exchange integral to the rigorous approach turned out to be within the analysis of the Curie temperature in the three-dimensional picture.

IV. CONCLUSIONS

The thermodynamic model of the //CrO_x(5 nm)/Co(t = 0.6, 0.7, 0.8, 0.9 nm)/Pt(2 nm) system is developed within the spin-wave approach, which consistently accounts for effects of non-two-dimensionality. For temperatures $T < 170 \pm 30$ K the temperature dependencies of the magnetization of the samples can be described well by the two-dimensional system (the term ΔM_0). Accounting for the transversal modes allows to fit the experimental data almost up to room temperature. However, only the lowest transversal mode ΔM_1 is relevant for the investigated samples and at room temperature its contribution is 7%–15%. For perpendicularly magnetized ultrathin ferromagnetic films interface-induced DMI has no influence on the magnetization temperature dependencies. Therefore, the fit of the $M(T)$ dependencies allows extraction of the important internal magnetic parameter, i.e., the exchange stiffness, without the need to know the DMI constant. The values of A extracted relying on the rigorous approach are about three times smaller compared to the bulk Co value. The 2D Bloch law can also be used for the determination of A. In this case, the fitting procedure should be performed in the temperature range $T < T_1$ (ΔM contains only a single-term ΔM_0). The exchange stiffness extracted from the 2D Bloch law, in this case, is practically the same as from the rigorous approach (the difference of A is about 5%–10%). The prediction of the exchange stiffness based on Bloch's $T^{3/2}$ law is about twice smaller than the result of the rigorous approach. The estimation of A from the Curie temperature within the 2D picture is sensitive to a specific model and overestimates values of the exchange stiffness (about two–six times) compared to the rigorous model. Very similar estimates for the exchange stiffness to the rigorous model are obtained based on the measurement of the Curie temperature of the ultrathin samples yet taking the proportionality coefficient in the scaling law as for bulk Co.

It is demonstrated that magnon thermodynamics can be successfully applied to access the exchange stiffness of technologically relevant ultrathin sandwiches featuring chiral magnetic interactions. The practical relevance for the thin-film magnetism community if far reaching. The developed approach enables the estimation of the exchange stiffness based on the technically simplistic measurement of the Curie temperature. Although demonstrated on the specific example of //CrO_x/Co/Pt trilayer stacks, the developed methodology is readily applicable to other systems independent of the layer stack. The important feature of the method is its applicability for the investigation of the thin films even with rather rough surfaces and high damping, where the methods based on dynamical approaches typically account difficulties. This versatility and simplicity of

the proposed approach suggests that the method has the potential to become a standard characterization tool in the community working in thin-film chiral magnetism.

Furthermore, the simple yet robust approach in the determination of the exchange stiffness is crucial not only for the experimental community. The exchange stiffness enters as the key parameter in all micromagnetic properties, including domain-wall width, period of the Dzyaloshinskii spiral, characteristic magnetic length. The determined exchange parameter of being about three times smaller compared to the bulk value has severe physical consequences both in statics and dynamics of magnetic textures. In combination with the rather strong magnetic anisotropy, this leads to a rather small characteristic length in this material of about 3 nm only. This suggests that the localized textures supported in these films can be extremely small of less than 10 nm. This is in stark contrast to the typical estimations in the community that the typical domain-wall width in Co/Pt-based systems is in the range of 20 nm. The smallness of the characteristic length is crucial as it potentially allows for large area density of skyrmion-based racetrack memory. From the point of view of magnetization dynamics, these thin films should exhibit higher viscosity for the motion of magnetic textures. Therefore, the possibility to assess this parameter is useful for the community working on the theory and micromagnetism of chiral magnetic textures in ultrathin asymmetrically sandwiched ferromagnetic films.

ACKNOWLEDGMENTS

This work is financed in part via the the German Research Foundation (DFG) Grants No. MA 5144/9-1, No. MA 5144/13-1, and No. MA 5144/14-1. I.A. Yastremsky is supported financially in the frame of the DAAD program "Research Stays for University Academics and Scientists, 2019". B.A. Ivanov is supported financially by the Program of NUST "MISiS" (Grant No. K2-2019-006), implemented by a governmental decree dated 16 March 2013, No. 211. We appreciate the assistance of A. Ponomaryov in the preparation of the FMR experiments.

APPENDIX A: CONVERGENCE TO BLOCH'S $T^{3/2}$ LAW

For sufficiently large film thicknesses, the sum in the expression for ΔM can be replaced by an integral $\Delta M =$

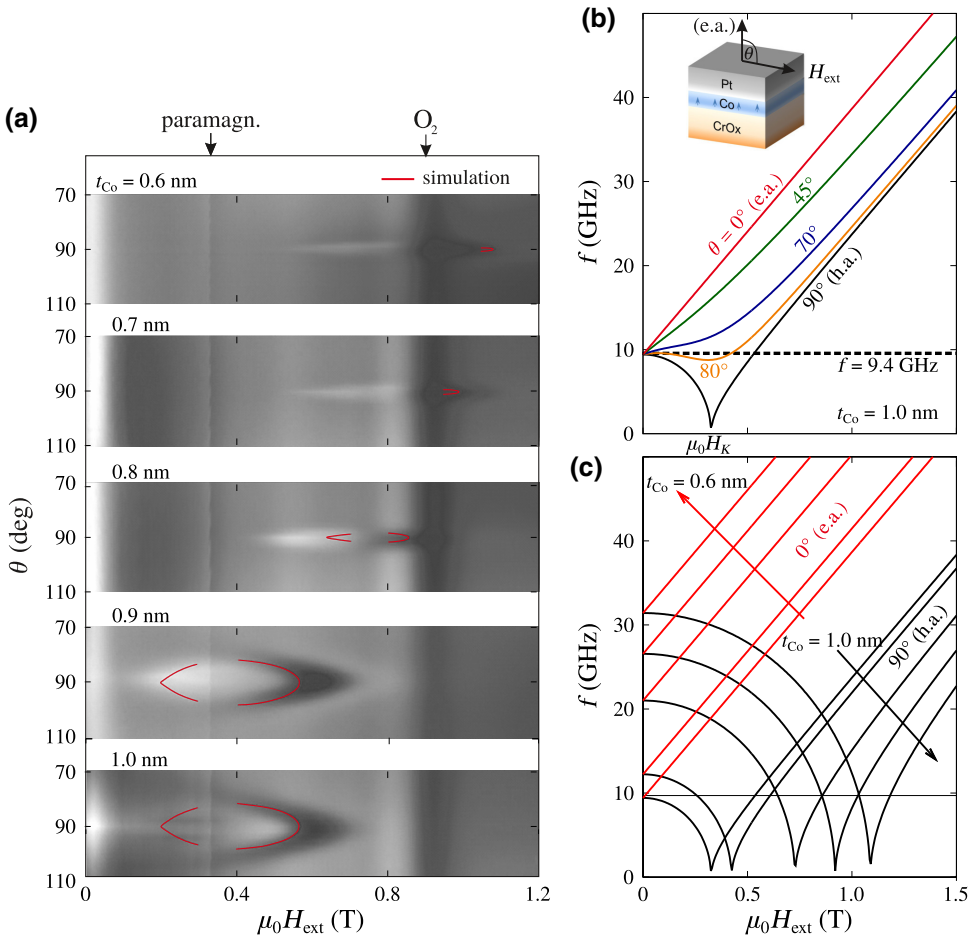

FIG. 3. (a) X-band FMR intensity map (derivative of absorption signal) of the angular dependence for the five Co thicknesses measured at $f = 9.4$ GHz. The position of the resonances agree with the calculations (red lines) based on the anisotropy fields H_K taken from the hysteresis loops. (b) Calculated frequency-field dependences of the resonances for various polar angles for the $//CrO_x/1.0$ nm Co/Pt trilayer. (c) Frequency-field dependencies for all samples at $\theta = 0°$ and 90°.

$\int_0^\infty D_{1D}\Delta M(\omega)d\omega$, where $D_{1D} = \frac{t}{2\sqrt{2}\pi}\sqrt{\frac{M}{\gamma A\omega}}$ is a one-dimensional spectral density of ΔM_{n_z} states. Integrating by parts, we restore Bloch's $T^{3/2}$ law [Eq. (4)].

APPENDIX B: FMR CHARACTERIZATION

Due to the low-amplitude and broad-line-width resonance signals of the samples, the FMR is measured using an X-band cavity at $f = 9.4$ GHz rather than using a broadband setup. The detected signals are only of the order of the O_2-resonance line from the surrounding air that is also detected by the cavity. Figure 3(a) maps the FMR absorption intensity on the external field and polar angle θ for the five different Co thicknesses. Resonances are only visible within a narrow angular range of up to $\pm 15^\circ$ around the hard axis. Figures 3(b) and 3(c) illustrate this feature. Figure 3(b) shows the calculated frequency-field dependencies of the //CrO_x/Co(1.0 nm)/Pt sample for several polar angles. The curves are calculated using Kittel's resonance equation, [41], i.e., for the field parallel to the easy axis, ($\theta = 0^\circ$):

$$f_{\text{res}} = \frac{\gamma\mu_0}{2\pi}\left(H_{\text{ext}} + M_{\text{eff}}\right), \tag{B1}$$

and for the field perpendicular to the easy axis ($\theta = 90^\circ$):

$$f_{\text{res}} = \frac{\gamma\mu_0}{2\pi}\sqrt{M_{\text{eff}}^2 - H_{\text{ext}}^2}, \quad \text{for } H_{\text{ext}} < M_{\text{eff}}, \tag{B2}$$

$$f_{\text{res}} = \frac{\gamma\mu_0}{2\pi}\sqrt{H_{\text{ext}}(H_{\text{ext}} - M_{\text{eff}})}, \quad \text{for } H_{\text{ext}} > M_{\text{eff}}. \tag{B3}$$

The effective magnetization $\mu_0 M_{\text{eff}}$ (anisotropy field) is obtained from the hard-axis loops. The horizontal dashed line denotes the FMR excitation frequency. Intersections, i.e., resonances, only exist for angles of about 80–90°. For the thinner samples, as depicted in Fig. 3(c), the zero-field resonance frequency increases to above 30 GHz for the thinnest sample. This shrinks down the angular range of possible resonances and shifts the resonances to higher resonance fields, as can be seen from the FMR maps. There are two intersections at $\theta = 90^\circ$, which correspond to the so-called unaligned resonance mode at lower fields (when $H_{\text{ext}} < M_{\text{eff}}$) and the uniform resonance mode at higher fields (when $H_{\text{ext}} > M_{\text{eff}}$). In the color maps they make up the black and white lobes. For the thin samples the overlap of the resonances with the oxygen resonances makes it impossible to retrieve an independent fit of the effective magnetization $\mu_0 M_{\text{eff}}$. For the thicker samples the amplitude of the unaligned resonances is too weak to be fitted properly—although still visible in the colormap. Hence, we adjust the FMR fits ($\mu_0 M_{\text{eff}}$) by the effective anisotropy taken from the hysteresis curves (H_K). The red curves are the corresponding calculations considering the gyromagnetic ratio of bulk Co ($\gamma = 1.92 \times 10^{11}$ rad/sT). As one can see the results agree. The remaining deviations can be explained by using a smaller gyromagnetic ratio of $\gamma = 1.63 \times 10^{11}$ rad/sT. This might be due to the influence of the CrO_x substrate. Hence, the effective anisotropy fields H_K obtained from the static investigations are verified.

APPENDIX C: THE IMPACT OF THE TEMPERATURE DEPENDENCE OF THE EXCHANGE STIFFNESS ON THE FITTING OF EXPERIMENTAL DEPENDENCIES $M(T)$

It is insightful to discuss the impact of the temperature dependence of the exchange stiffness on the fitting of the experimental $M(T)$ data [42–44]. To account for this effect in the developed model, the exchange stiffness is presented as $A(T) = A[M(T)/M(0)]^\kappa$, where the unknown parameters are the exchange stiffness A at $T = 0$ K and

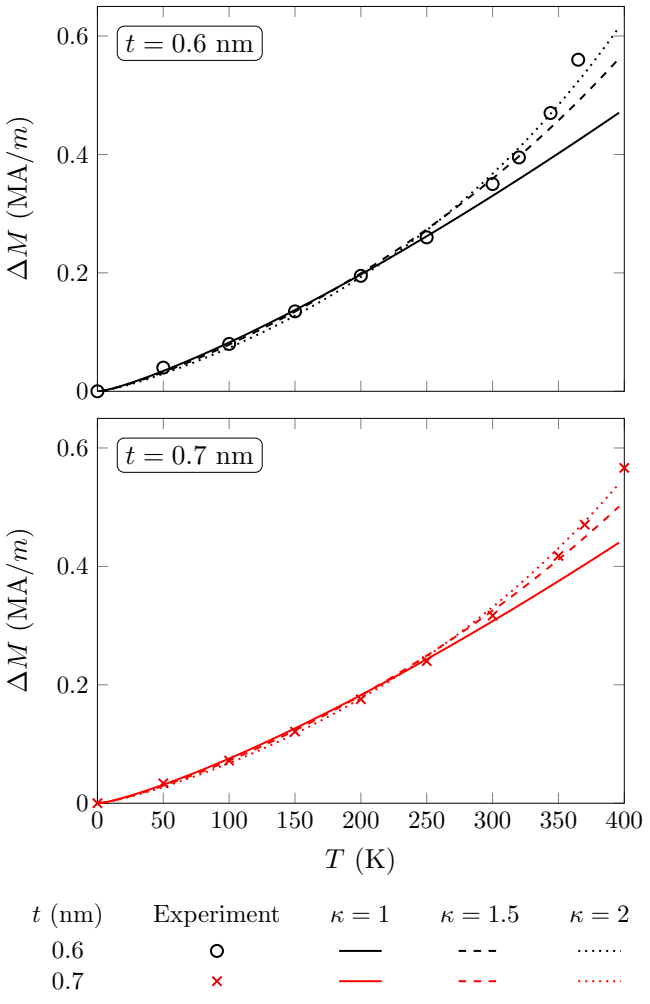

FIG. 4. Experimental (symbols) and theoretical (lines) temperature dependencies of ΔM for $t = 0.6$, 0.7 nm and different scaling exponents $\kappa = 1, 1.5, 2$.

the scaling exponent κ. The exact value of the scaling exponent κ depends on the system parameters, in particular on the number of neighbors and the strength of the anisotropy [42]. The prediction of the mean-field theory gives $\kappa = 2$. For the temperature dependence of the Heisenberg exchange stiffness of 3D magnets κ is calculated to be between 1.66 and 1.76 [42]. For a monolayer ferromagnetic film $\kappa \approx 1.54 - 1.57$ [44]. When estimating A in the Table II, M and A are taken at $T = 0$, as in the original derivation of Bloch's $T^{3/2}$ law [33,41]. This situation is equivalent to $\kappa = 1$. At low temperatures, when $\Delta M/M$ is small, $M(T)$ dependencies are practically independent of the scaling exponent κ. Therefore, typical values of $\kappa = 1,\ 1.5,\ 2$ are taken and the exchange stiffness A is supposed to be the only fitting parameter. The fit is performed in a way to maximally extend the temperature range of an agreement between the experimental data and theory.

Figure 4 demonstrates the result of this fitting procedure for the $M(T)$ data taken of the samples with $t = 0.6$ and 0.7 nm. The best fit for $\kappa = 1$ allows the experimental $M(T)$ data to be described with a standard deviation of 2–3% up to 250 K for both samples. For the two-dimensional prediction with $\kappa = 1.5$, the experimental data can be fitted up to higher temperatures of 320–350 K for $t = 0.6$ and 0.7 nm, however the standard deviation is 3%. For the mean-field prediction with $\kappa = 2$, the experimental data can be fitted up to 340 K ($t = 0.6$ nm) and 400 K ($t = 0.7$ nm), yet with the accuracy of 4%–5%. The extracted value of A increases by about 6% for $\kappa = 1.5$ and by about 17% for $\kappa = 2$ compared to the values for $\kappa = 1$ (Table II, the column indicated as "Rig. appr."). Thus, all tested values of the critical exponent $\kappa = 1,\ 1.5,\ 2$ provide reasonable agreement with the experimental data. However, it is impossible unambiguously to chose which tested value of κ better describes the experimental data. This ambiguity indicates that for temperatures higher than room temperature additional effects (like a discreteness of a crystal lattice in the spin-wave dispersion law, nonlinear effects) should also be accounted for [45].

[1] A. Fert, V. Cros, and J. Sampaio, Skyrmions on the track, Nat. Nanotechnol. **8**, 152 (2013).

[2] D. Sander, S. O. Valenzuela, D. Makarov, C. H. Marrows, E. E. Fullerton, P. Fischer, J. McCord, P. Vavassori, S. Mangin, P. Pirro, B. Hillebrands, A. D. Kent, T. Jungwirth, O. Gutfleisch, C. G. Kim, and A. Berger, The 2017 magnetism roadmap, J. Phys. D: Appl. Phys. **50**, 363001 (2017).

[3] R. Wiesendanger, Nanoscale magnetic skyrmions in metallic films and multilayers: A new twist for spintronics, Nat. Rev. Mater. **1**, 16044 (2016).

[4] W. Jiang, P. Upadhyaya, W. Zhang, G. Yu, M. B. Jungfleisch, F. Y. Fradin, J. E. Pearson, Y. Tserkovnyak, K. L. Wang, O. Heinonen, S. G. E. te Velthuis, and A. Hoffmann, Blowing magnetic skyrmion bubbles, Science **349**, 283 (2015).

[5] A. Thiaville, S. Rohart, E. Jue, V. Cros, and A. Fert, Dynamics of Dzyaloshinskii domain walls in ultrathin magnetic films, Europhys. Lett. **100**, 57002 (2012).

[6] C. Moreau-Luchaire, C. Moutafis, N. Reyren, J. Sampaio, C. A. F. Vaz, N. Van Horne, K. Bouzehouane, K. Garcia, C. Deranlot, P. Warnicke, P. Wohlhüter, J.-M. George, M. Weigand, J. Raabe, V. Cros, and A. Fert, Additive interfacial chiral interaction in multilayers for stabilization of small individual skyrmion at room temperature, Nat. Nanotechnol. **11**, 444 (2016).

[7] O. Boulle, *et al.*, Room-temperature chiral magnetic skyrmions in ultrathin magnetic nanostructures, Nat. Nanotechnol. **11**, 449 (2016).

[8] A. Spinelli, B. Bryant, F. Delgado, J. Fernndez-Rossier, and A. F. Otte, Imaging of spin waves in atomically designed nanomagnets, Nat. Mater. **13**, 782 (2014).

[9] R. Vollmer, M. Etzkorn, P. S. A. Kumar, H. Ibach, and J. Kirschner, Spin-Polarized Electron Energy Loss Spectroscopy of High Energy, Large Wave Vector Spin Waves in Ultrathin fcc Co Films on Cu(001), Phys. Rev. Lett. **91**, 147201 (2003).

[10] T. Devolder, J.-V. Kim, L. Nistor, R. Sousa, B. Rodmacq, and B. Diény, Exchange stiffness in ultrathin perpendicularly magnetized CoFeB layers determined using the spectroscopy of electrically excited spin waves, J. Appl. Phys. **120**, 183902 (2016).

[11] H. A. Alperin, O. Steinsvoll, G. Shirane, and R. Nathans, Observation of the dispersion relation for spin waves in hexagonal cobalt, J. Appl. Phys. **37**, 1052 (1966).

[12] V. V. Kruglyak, A. Barman, R. J. Hicken, J. R. Childress, and J. A. Katine, Processional dynamics in microarrays of nanomagnets, J. Appl. Phys. **97**, 10A706 (2005).

[13] V. V. Kruglyak, A. Barman, R. J. Hicken, J. R. Childress, and J. A. Katine, Picosecond magnetization dynamics in nanomagnets: Crossover to nonuniform precession, Phys. Rev. B **71**, 220409(R) (2005).

[14] M. Mulazzi, A. Chainani, Y. Takata, Y. Tanaka, Y. Nishino, K. Tamasaku, T. Ishikawa, T. Takeuchi, Y. Ishida, Y. Senba, H. Ohashi, and S. Shin, Temperature dependence of the exchange stiffness in FePd(001) thin films: Deviation from the empirical law $A(T) \propto M_S^2$ at intermediate temperatures, Phys. Rev. B **77**, 224425 (2008).

[15] X. Liu, M. M. Steiner, R. Sooryakumar, G. A. Prinz, R. F. C. Farrow, and G. Harp, Exchange stiffness, magnetization, and spin waves in cubic and hexagonal phases of cobalt, Phys. Rev. B **53**, 12166 (1996).

[16] C. Bilzer, T. Devolder, J.-V. Kim, G. Counil, C. Chappert, S. Cardoso, and P. P. Freitas, Study of the dynamic magnetic properties of soft CoFeB films, J. Appl. Phys. **100**, 053903 (2006).

[17] M. Langer, K. Wagner, T. Sebastian, R. Hubner, J. Grenzer, Y. T. Wang, T. Kubota, T. Schneider, S. Stienen, K. Lenz, H. Schultheiss, J. Lindner, K. Takanashi, R. E. Arias, and J. Fassbender, Parameter-free determination of the exchange constant in thin films using magnonic patterning, Appl. Phys. Lett. **108**, 102402 (2016).

[18] N. Romming, A. Kubetzka, C. Hanneken, K. von Bergmann, and R. Wiesendanger, Field-Dependent Size and Shape of Single Magnetic Skyrmions, Phys. Rev. Lett. **114**, 177203 (2015).

[19] S. Okamoto, N. Kikuchi, O. Kitakami, T. Miyazaki, Y. Shimada, and K. Fukamichi, Chemical-order-dependent magnetic anisotropy and exchange stiffness constant of FePt (001) epitaxial films, Phys. Rev. B **66**, 024413 (2002).

[20] N. Sato, R. M. White, and S. X. Wang, Effect of annealing on exchange stiffness of ultrathin CoFeB film with perpendicular magnetic anisotropy, Appl. Phys. Lett. **108**, 152405 (2016).

[21] The complete micromagnetic characterization of asymmetrically sandwiched ferromagnetic films, arXiv preprint at https://arxiv.org/abs/1706.09322.

[22] U. Krey, On the significance of quantum effects and interactions for the apparent universality of Bloch laws $M_S(T)$, J. Magn. Magn. Mater. **268**, 277 (2004).

[23] W. Kipferl, M. Dumm, P. Kotissek, F. Steinbauer, and G. Bayreuther, Bloch's law for epitaxial ultrathin dot arrays with uniaxial magnetic anisotropy, J. Appl. Phys. **95**, 7417 (2004).

[24] S. Cojocaru, A. Naddeo, and R. Citro, Modification of the Bloch law in ferromagnetic nanostructures, EPL **106**, 17001 (2014).

[25] P. M. Shepley, H. Tunnicliffe, K. Shahbazi, G. Burnell, and T. A. Moore, Magnetic properties, domain-wall creep motion, and the Dzyaloshinskii-Moriya interaction in Pt/Co/Ir thin films, Phys. Rev. B **97**, 134417 (2018).

[26] H. T. Nembach, J. M. Shaw, M. Weiler, E. Ju, and T. J. Silva, Linear relation between Heisenberg exchange and interfacial Dzyaloshinskii–Moriya interaction in metal films, Nat. Phys. **11**, 825 (2015).

[27] A. Thiaville, S. Rohart, E. Jué, V. Cros, and A. Fert, Dynamics of Dzyaloshinskii domain walls in ultrathin magnetic films, EPL **100**, 57002 (2012).

[28] C. E. Zaspel, T. E. Grigereit, and J. E. Drumheller, Soliton Contribution to the Electron Paramagnetic Resonance Linewidth in the Two-Dimensional Antiferromagnetic, Phys. Rev. Lett. **74**, 4539 (1995).

[29] C. E. Zaspel and J. E. Drumheller, Electron paramagnetic resonance detection of solitons in two-dimensional magnets, Int. J. Mod. Phys. B, **10**, 3649 (1996).

[30] S. Pizzini, J. Vogel, S. Rohart, L. D. Buda-Prejbeanu, E. Jué, O. Boulle, I. M. Miron, C. K. Safeer, S. Auffret, G. Gaudin, and A. Thiaville, Chirality-Induced Asymmetric Magnetic Nucleation in Pt/Co/AlOx Ultrathin Microstructures, Phys. Rev. Lett. **113**, 047203 (2014).

[31] J. Cho, N.-H. Kim, S. Lee, J.-S. Kim, R. Lavrijsen, A. Solignac, Y. Yin, D.-S. Han, N. J. J. van Hoof, H. J. M. Swagten, B. Koopmans, and C.-Y. You, Thickness dependence of the interfacial Dzyaloshinskii–Moriya interaction in inversion symmetry broken systems, Nat. Commun. **6**, 7635 (2015).

[32] M. Belmeguenai, J.-P. Adam, Y. Roussigné, S. Eimer, T. Devolder, J.-V. Kim, S. M. Cherif, A. Stashkevich, and A. Thiaville, Interfacial Dzyaloshinskii-Moriya interaction in perpendicularly magnetized Pt/Co/AlOx ultrathin films measured by Brillouin light spectroscopy, Phys. Rev. B **91**, 180405(R) (2015).

[33] F. Bloch, Zur Theorie des Ferromagnetismus, Z. Phys. **61**, 206 (1930).

[34] M. J. Klein and R. S. Smith, Thin ferromagnetic films, Phys. Rev. **81**, 378 (1951).

[35] R. P. Erickson and D. I. Mills, Thermodynamics of thin ferromagnetic films in the presence of anisotropy and dipolar coupling, Phys. Rev. B **44**, 11825 (1991).

[36] N. D. Mermin and H. Wagner, Absence of Ferromagnetism or Antiferromagnetism in One- or Two-Dimensional Isotropic Heisenberg Models, Phys. Rev. Lett. **17**, 1133 (1966).

[37] L. D. Landau and E. M. Lifshitz, *Course of Theoretical Physics – Volume 5: Statistical Physics, Part 1* (Elsevier, Butterworth-Heinemann, New York, 1980), 3rd ed.

[38] P. Bruno, Magnetization and Curie temperature of ferromagnetic ultrathin films: The influence of magnetic anisotropy and dipolar interactions, Mater. Res. Soc. Symp. Proc. **231**, 299 (1992).

[39] P. E. Tannenwald and R. Weber, Exchange integral in cobalt from spin-wave resonance, Phys. Rev. **121**, 715 (1961).

[40] P. J. Metaxas, J. P. Jamet, A. Mougin, M. Cormier, J. Ferré, V. Baltz, B. Rodmacq, B. Dieny, and R. L. Stamps, Creep and Flow Regimes of Magnetic Domain-Wall Motion in Ultrathin Pt/Co/Pt Films with Perpendicular Anisotropy, Phys. Rev. Lett. **99**, 217208 (2007).

[41] C. Kittel, *Introduction to Solid State Physics* (Wiley, New York, 2004), 8th ed.

[42] U. Atxitia, D. Hinzke, O. Chubykalo-Fesenko, U. Nowak, H. Kachkachi, O. N. Mryasov, R. F. Evans, and R. W. Chantrell, Multiscale modeling of magnetic materials: Temperature dependence of the exchange stiffness, Phys. Rev. B **82**, 134440 (2010).

[43] R. Moreno, R. F. L. Evans, S. Khmelevskyi, M. C. Muñoz, R. W. Chantrell, and O. Chubykalo-Fesenko, Temperature-dependent exchange stiffness and domain wall width in Co, Phys. Rev. B **94**, 104433 (2016).

[44] L. Rózsa, U. Atxitia, and U. Nowak, Temperature scaling of the Dzyaloshinsky-Moriya interaction in the spin wave spectrum, Phys. Rev. B **96**, 094436 (2017).

[45] F. Dyson, Thermodynamic behavior of an ideal ferromagnet, Phys. Rev. **102**, 1230 (1956).